

Barely visible impact damage identification in a 3D core sandwich structure

Shirsendu Sikdar, Wiesław Ostachowicz, Paweł Kudela,
Maciej Radziński
*Institute of Fluid-Flow Machinery
Polish Academy of Sciences
Fiszera 14, 80-231 Gdansk, Poland
e-mail: ssikdar@imp.gda.pl, wieslaw@imp.gda.pl, pk@imp.gda.pl,
maciej.radzienski@imp.gda.pl*

3D core sandwich structure (3DCSS) is a popular lightweight construction material in the automotive, aerospace and marine industries. However, barely visible low-speed impact-damage (BVLID) may occur in the 3DCSS due to foreign-object-impact that can significantly reduce the load-bearing capacity of the structure. This paper presents a guided wave (GW) propagation based BVLID identification technique for the 3DCSS. A global-matrix formulation based semi-analytical model is applied to generate the dispersion curve for the GW propagation in the 3DCSS. It is observed that the GW propagation in the 3DCSS is multi-modal in nature. Finite-element numerical simulation of GW propagation in the 3DCSS is carried out in Abaqus. A significant increment in the primary antisymmetric mode is noticed due to the presence of BVLID region in the structure. Experiments are then conducted on a 3DCSS sample to validate the simulation results. There is a good agreement between the simulation and experimental results in all the cases.

Keywords: 3D core sandwich structure, dispersion curve, barely visible impact damage, guided wave.

1. INTRODUCTION

Sandwich composite structures have proven their usefulness as lightweight construction materials in the aerospace, aeronautics, automotive, marine and civil engineering structures [6]. The 3DCSS is a recent concept of sandwich construction, in which glass-fiber composite face-sheets are bonded to the top and bottom surface of a hexagonal honeycomb composite core with epoxy adhesive [27]. The combination of thick-core and thin-skins with higher stiffness results in a strong and lightweight structure. However, low speed impacts can cause barely visible localized damage or disbonds (e.g., BVLIDs) at the core-skin interphase, which may in turn cause a serious loss in stiffness and may jeopardize the safety and integrity of the structural assembly [5]. Therefore, detection of such BVLIDs is important to prevent failures of such structure.

An experimental and analytical impact-damage study on a loaded sandwich fuselage keel panel was presented by Mikulik in [14]. It was concluded that the low-speed impact damage depends on the impact energy and the velocity of the impactor. There have been many attempts to study the barely visible impact damage characteristics and to develop identification techniques to assess different types of damage [9, 19, 20, 22].

The guided Lamb wave-based inspection methods have the potential to detect defects in sandwich structures [7, 8, 12, 15, 18]. The major referred advantages of the ultrasonic guided Lamb wave-based BVLID inspection techniques are their potential to penetrate into the hidden layers, the long distance inspection capability, and the resulting modification in wave packets based on

their frequency and phase-velocity [11, 17]. It was also suggested that the identification of different GW modes is essential for the success of GW-based structural health monitoring (SHM) and non-destructive evaluation (NDE) of composites using piezoelectric transducers [13, 28]. The complex nature of composite sandwich structures imposes many challenges for the understanding of GW propagation characteristics with different operating frequencies [2]. The GW propagation phenomenon in honeycomb sandwich structures using bonded piezoelectric transducers was investigated by Song, Huang and Hudson in [25]. Many authors [7, 8, 27] have demonstrated a significant amplification in GW mode amplitudes due to presence of debonding in sandwich composite structures. A received sensor-signal input-based debonding detection algorithm for sandwich composite structures was proposed by Mustapha and Ye [15]. Sikdar et al. [23] proposed a baseline-free damage detection algorithm to assess the face-sheet-core debondings in a honeycomb composite sandwich structures, using a piezoelectric sensor network.

Theoretical studies on GW propagation in sandwich composite structures with the aim to investigate the dispersion phenomenon of the propagating guided Lamb waves attributable to transient excitation were also proposed in [1, 16, 21, 26]. Two-dimensional (2D) theoretical models with limited applications were developed for guided Lamb wave propagation in sandwich structures and presented in [4, 7, 10]. A global matrix method-based 2D robust semi-analytical GW propagation model for fast calculations of dispersion curves in laterally unbounded sandwich composites was presented by Banerjee and Pol in [3]. Their semi-analytical model has proven to be capable of accurately analyzing the propagating GW mode characteristics in a triple-layered sandwich composite structure. However, guided Lamb wave propagation and BVLID detection in 3DCSS have not been studied yet and remain open for the investigation.

In this research paper, a theoretical dispersion curve is obtained for ultrasonic guided Lamb wave propagation in the 3DCSS. Based on the dispersion curve, different wave modes in the experimentally and numerically obtained sensor signals are efficiently identified.

A 3D finite element (FE) simulation of wave propagation in the 3DCSS in presence of the BVLID region is carried out in ABAQUS. Laboratory experiments are then conducted to verify the FE simulation results, and to detect the BVLID region within an optimized array of piezoelectric transducer disks (PTDs). The differential features in the BVLID induced sensor signals are captured by applying a probability-based signal difference algorithm, which uses an image-fusion strategy to visualize the possible BVLID region in the 3DCSS.

2. EXPERIMENTAL SETUP

An experimental setup was configured in the laboratory to carry out the inspection of 3DCSS using a network of PTDs. The following sub-sections explain in detail the experimental setups based on ultrasonic guided Lamb wave propagation

2.1. 3DCSS sample plate and experimental setup

A hexagonal epoxy honeycomb foam core (3D-core) and glass fiber reinforced face-sheet made of 3DCSS ($500 \times 500 \times 7$ mm) sample is selected for the experiment, as shown in Fig. 1. The elastic properties of the triple-layered 3DCSS are shown in Table 1. A BVLID region is introduced into the sample plate by using a standard steel ball-drop impact device with impact energy of 10 J. The visual appearance of the impacted zone is measured to be a circularshaped region with approximately 15 mm in diameter. The NCE51 circular PTDs (10 mm diameter and 0.4 mm thickness) are applied for the actuation and reception of propagating ultrasonic GW signals in the 3DCSS.

The PTDs are efficiently operated by a multi-channel function-generator (FGEN) cum data-acquisition (DAQ)-based PXI-system, and a computer to control the PXI-system and to save the required sensor data. The experimental setup is shown in Fig. 2.

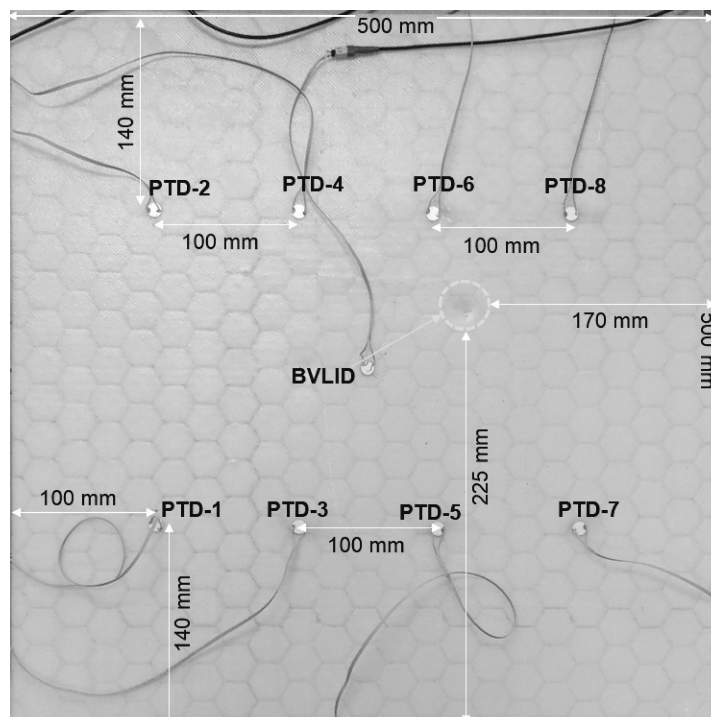


Fig. 1. Experimental sample 3DCSS plate.

Table 1. 3DCSS elastic properties.

Material	E_1 [GPa]	E_2 [GPa]	E_3 [GPa]	G_{12} [GPa]	G_{23} [GPa]	G_{13} [GPa]	ν_{12}	ν_{13}	ν_{23}	ρ [kg/m ³]	t [mm]
Face-sheet	30.35	30.35	5.9	12.42	3.66	3.66	0.05	0.26	0.26	2400	1
3D core	1.45	1.45	2.33	0.088	0.172	0.172	0.42	0.42	0.42	78	5
Adhesive	0.0486	0.0486	0.0486	0.0174	0.0174	0.0174	0.40	0.40	0.40	125	0.05

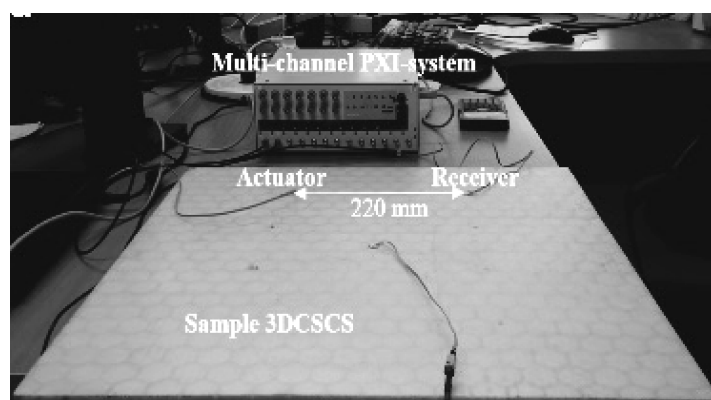


Fig. 2. Experimental setup for operating frequency modulation of the PTDs.

2.2. Selection of an optimized PTD operating signal

An optimum driving frequency of the PTDs is determined by placing two PTDs (actuator and sensor) on the sample 3DCSS at a distance of 220 mm (Fig. 2). In this process, a range of actuator driving frequencies is applied and the corresponding GW signals are collected from the sensor.

The collected GW signals are then analyzed to determine maximum modal responses for different driving frequencies and a frequency-response graph is plotted (Fig. 3a). It is noticed that the sensor signals are showing highest response at around 100 kHz frequency. Therefore, a 100 kHz 5-cycle sine pulse in a Hanning window (Fig. 3b) is selected as actuation frequency for all the cases, unless stated otherwise.

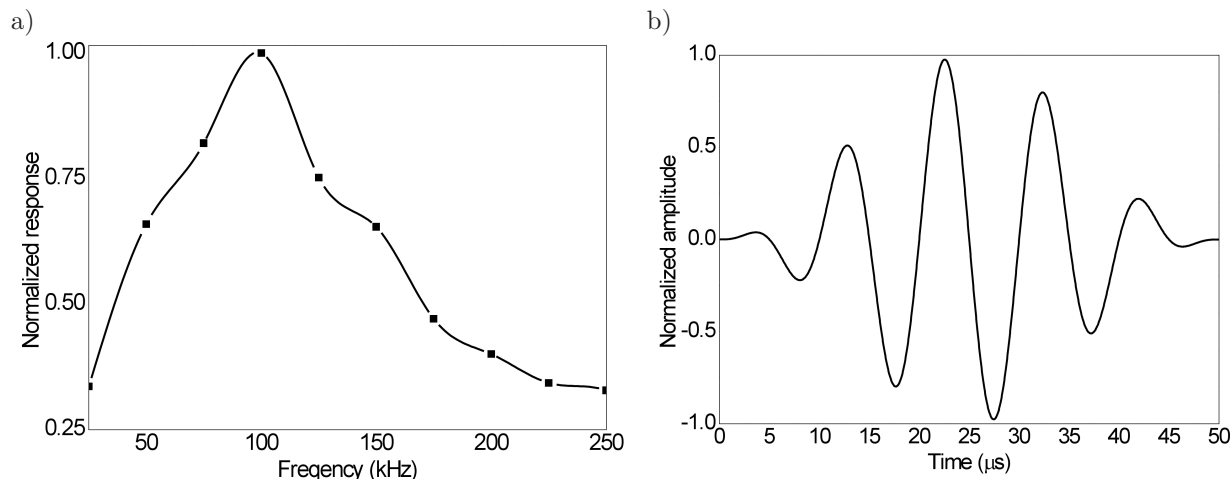


Fig. 3. a) PTD calibration curve for frequency modulation, b) selected 100 kHz input signal.

3. FE SIMULATION

Owing to the complexities involved in the geometry and the boundary conditions, analytical prediction of BVLID influences on the GWs in the damaged 3DCSS is difficult. Thus, the BVLID influences on the propagating GW modes are numerically studied using the FE simulation in ABAQUS. In the simulation, the sample 3DCSS ($500 \times 500 \times 7$ mm) plate is modeled using the Abaqus explicit-code and the PTDs (10 mm diameter and 0.4 mm thin) are modeled using the Abaqus implicit-code. The “standard explicit co-simulation technique” is used to correlate the explicit and the implicit analysis of wave propagation in the 3DCSS [24].

In the explicit modeling of 3DCSS, the eight-noded C3D8R linear brick elements (hourglass control and reduced integration) are used. To model the zero-volume circular BVLID region the element nodes are demerged (resembling debonding type of impact damage) at the adhesive-face sheet and the 3D core-adhesive interphase, as shown in Fig. 4. Different element sizes are considered for different layers, such as: face-sheet: $0.5 \times 0.5 \times 0.245$ mm, 3D-core: $0.5 \times 0.5 \times 0.25$ mm, and adhesive: $0.5 \times 0.5 \times 0.01$ mm. In the implicit code, the PTDs (actuator/sensor) are modeled using the eight-noded standard C3D8E linear piezoelectric brick elements with six degrees of freedoms at each node. The selected input signal as voltage is applied to the top-surface nodes of the actuator PTDs, and zero voltage is assigned to the bottom-surface nodes of the actuator and sensor-PTDs for the grounding-operation. The output signal is recorded at the top-surface of the sensor-PTDs. In the FE simulation, the NCE51 PTD material properties are assumed as per the manufacturer’s information as

$$[c] = \begin{bmatrix} 13.4 & 8.89 & 9.09 & 0 & 0 & 0 \\ & 13.4 & 9.09 & 0 & 0 & 0 \\ & & 12.1 & 0 & 0 & 0 \\ & & & 2.05 & 0 & 0 \\ & & & & 2.05 & 0 \\ & & & & & 2.24 \end{bmatrix} \times 10^{10} \text{ N/m}^2,$$

Symmetry

$$[\varepsilon] = \begin{bmatrix} 1.72 & 0 & 0 \\ & 1.72 & 0 \\ & \text{Symmetry} & 1.68 \end{bmatrix} \times 10^{-8} \text{ C/Vm},$$

$$[e] = \begin{bmatrix} 0 & 0 & 0 & 0 & 13.7 & 0 \\ 0 & 0 & 0 & 13.7 & 0 & 0 \\ -6.06 & -6.06 & 17.2 & 0 & 0 & 0 \end{bmatrix} \text{ C/m}^2,$$

where $[c]$ represents the mechanical stiffness matrix, $[\varepsilon]$ represents the piezoelectric permittivity matrix, and $[e]$ represents the piezoelectric stress matrix. The piezoelectric material density (ρ) is assumed as 7800 kg/m^3 .

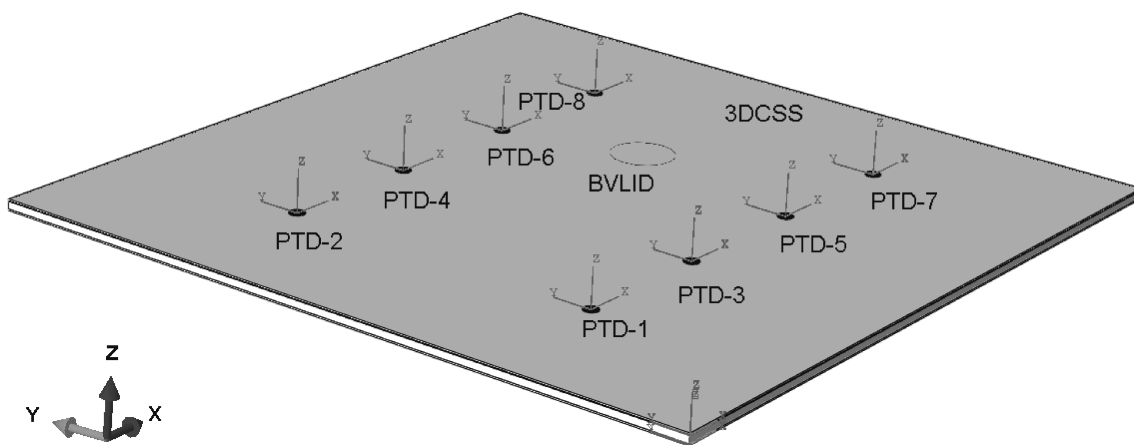


Fig. 4. FE-based numerical model of 3DCSS with PTDs in Abaqus.

4. RESULTS AND DISCUSSION

4.1. Dispersion curve and BVLID effects

A global-matrix method-based semi-analytical model is used to obtain the theoretical frequency versus the phase velocity dispersion curve for the 3DCSS. Detailed formulation of the semi-analytical model can be found in [3] and hence, the same will not be repeated here for brevity. The 2D semi-analytical formulation is ultimately summarized into a 12×12 global-matrix form for a three layer structure, and dispersion condition is obtained by solving the determinant of the global matrix as

$$G(\xi_1, \omega) = 0. \quad (1)$$

The real values of wavenumber ξ_1 can be obtained for the known values of frequency ω , and the corresponding dispersion plots can be obtained by using

$$c_p = \frac{\omega}{\xi_1}, \quad (2)$$

where c_p represent the phase-velocity of the ultrasonic guided Lamb wave modes.

Thus, the dispersion curve is obtained for the 3DCSS as shown in Fig. 5.

Based on the dispersion curve in Fig. 5, the presence of different wave modes (A0, S0, A1 and S1) is identified in the healthy simulated signal presented in Fig. 6. The simulated signal corresponding

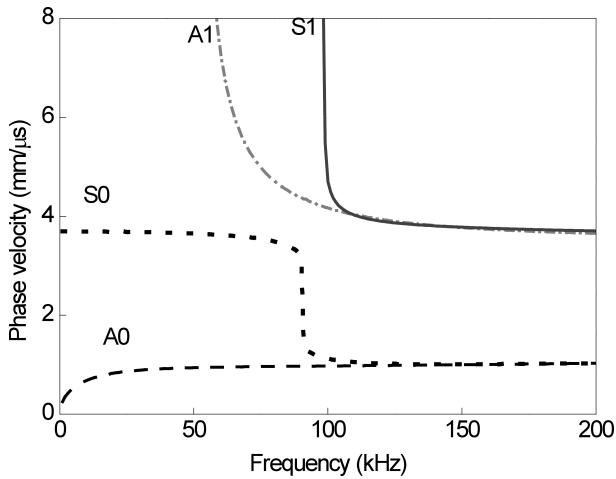


Fig. 5. Dispersion curve of GW propagation in the DCSS.

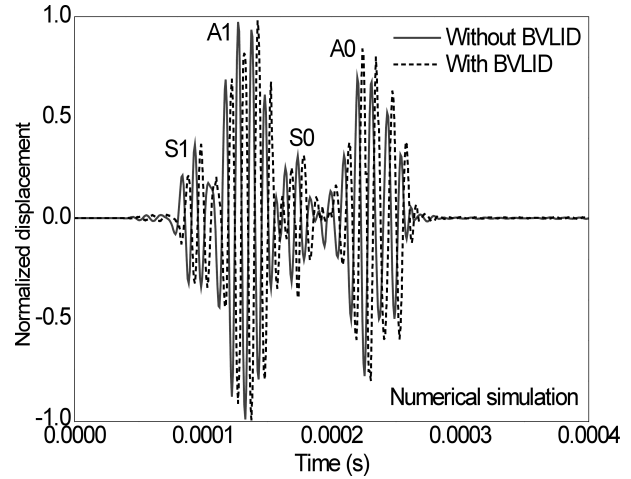


Fig. 6. Comparison of numerical time-history responses for cases with and without BVLID

to the actuator-sensor path: 1-2 (Fig. 4) is considered as the baseline signal since this path is considerably away from the BVLID regions.

The BVLID-influenced signal is collected from the actuator-sensor path: 3-4, which is across the BVLID. The BVLID signal is then compared with the healthy signal, which shows a significant amplification of the primary anti-symmetric (A0) mode in the BVLID signal, as shown in the Fig. 6.

Similarly, the healthy experimental GW signal from PTD path: 1-2 (Fig. 1) is obtained and compared with the healthy simulation signal, as shown in Fig. 7. The comparison shows a good agreement between the FE simulation and the experiment.

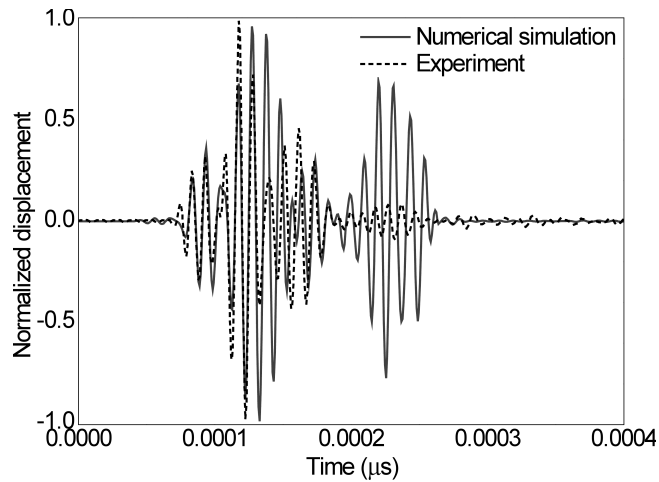


Fig. 7. Comparison of numerical and experimental healthy signals.

The experimental BVLID-influenced sensor signal is then collected from the actuator-sensor path: 3-4, which is across the BVLID (Fig. 1). The comparison between the healthy and the BVLID experimental signal is shown in Fig. 8a, which implies that the presence of BVLID in the 3DCSS significantly influences the GW signals, in terms of amplification of the A0-mode. The Hilbert transform (HT) of the experimental GW signals in Fig. 8a is presented in Fig. 8b, which represents the BVLID effect on the A0-mode amplitude.

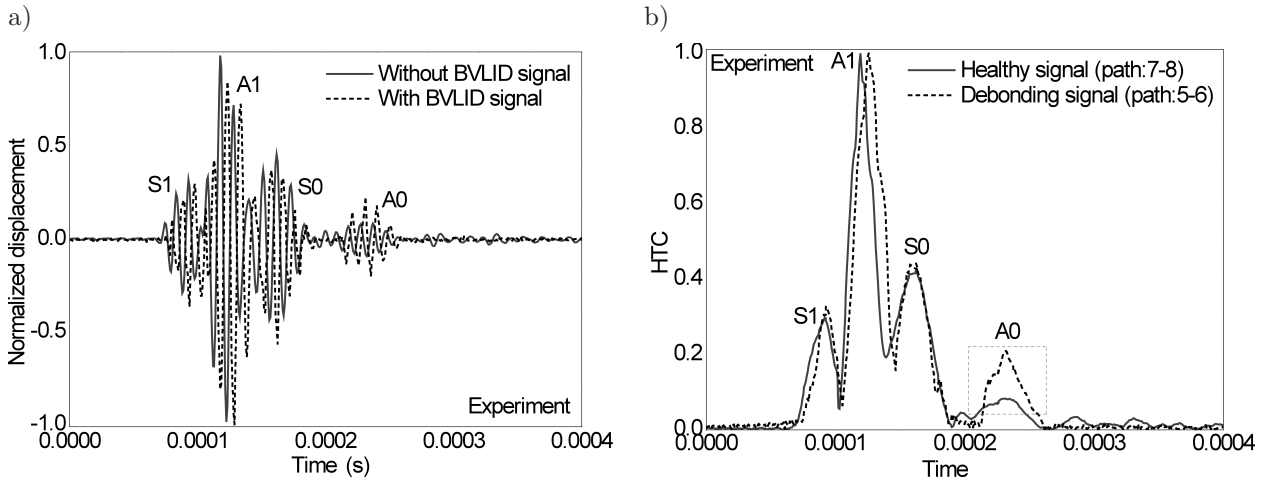


Fig. 8. a) Comparison of experimental time-history responses for cases with and without BVLID, b) HT of the signals in Fig. 7a.

4.2. Detection of BVLID region in the 3DCSS

A signal difference algorithm is applied to identify the BVLID regions in the 3DCSS. The HT of the experimental sensor signals in time-domain (e.g. Fig. 8b) is used for characterization of BVLID-influences on the GW modes in the sensor signals. In order to capture the differential characteristics of BVLID, the signal difference coefficients are obtained by comparing the A0 mode amplitudes of the transformed time-domain receiver signals. The probability distribution of BVLID is computed to visualize the damaged region by applying the extracted signal difference coefficients as input to each pixel. The image quality is improved by using an image fusion technique. The BVLID localization indicator K_d of any random position (x, y) within the sensor network can be described as [29]

$$K_d(x, y) = \sum_{i=1}^{N-1} \sum_{j=i+1}^N D_{ij}(x, y) = \sum_{i=1}^{N-1} \sum_{j=i+1}^N S_{ij}(x, y) \left[\frac{\psi - R_{ij}(x, y)}{\psi - 1} \right], \quad (3)$$

where, $D_{ij}(x, y)$ is the BVLID-distribution probability, measured from the actuator-sensor pair: $i-j$ and $S_{ij}(x, y)$ represents the signal difference coefficient, which is the difference in amplitude area between signals with and without BVLID for a particular GW mode. The signal difference coefficient can be expressed as

$$S_{ij} = \sqrt{\frac{\int_{t_1}^{t_2} (s^b - s^h) dt}{\int_{t_1}^{t_2} [s^b]^2 dt}}, \quad (4)$$

where s^b and s^h represent the signals with and without BVLID, t_1 is the time of arrival of A0 mode in the signal and $t_2 = (t_1 + \text{temporal duration of the A0 mode})$, $\left[\frac{\psi - R_{ij}(x, y)}{\psi - 1} \right]$ is an elliptical contour-shaped spatial distribution function with nonnegative values, where

$$R_{ij}(x, y) = \begin{cases} D_{ij}(x, y), & L_{ij}(x, y) < \psi, \\ \psi, & L_{ij}(x, y) \geq \psi, \end{cases} \quad (5)$$

where

$$L_{ij}(x, y) = \frac{(\sqrt{(x - x_i)^2 + (y - y_i)^2} + \sqrt{(x - x_j)^2 + (y - y_j)^2})}{l_{ij}}, \quad (6)$$

where l_{ij} represents the distance between actuator “ i ” and sensor “ j ”, and ψ is the small scaling parameter, which reduces the size of the BVLID region and it is independent of propagating signal velocity. The magnitude of ψ is calculated empirically and, in this study, it is assumed as 1.05 [29].

Based on the change in amplitude of the A0 mode owing to the presence of BVLID region, the signal difference algorithm in MATLAB is applied to capture the unknown BVLID regions in the 3DCSS. The algorithm uses the HT of the received GW signals (e.g., Fig. 8b) collected experimentally from the PTD sensor network (Fig. 1). The magnitude of BVLID index (signal difference coefficient magnitudes) at every pixel is obtained by processing the received signals from the actuator-sensor path: 1-2, 3-4, 5-6, 7-8, 1-8, 2-7, and plotted in Fig. 9. The BVLID index maps in grid pattern (Fig. 9a) and contour pattern (Fig. 9b) clearly show the BVLID zone in the sample 3DCSS, corresponding to the higher BVLID index magnitudes.

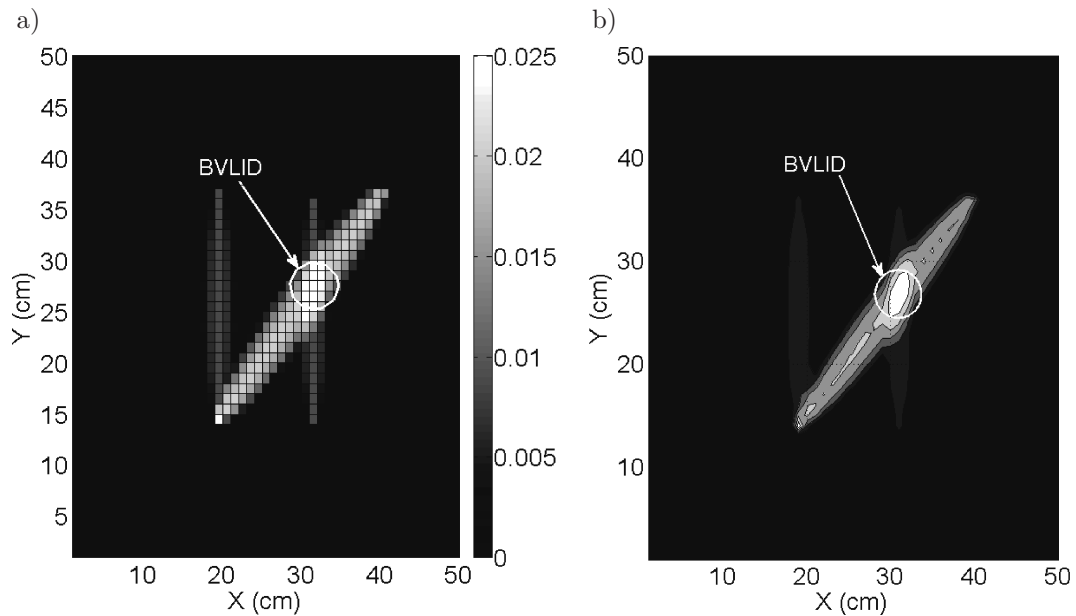


Fig. 9. BVLID index maps in a) grid and b) contour pattern showing the location of BVLID.

5. CONCLUSIONS

Dispersion of the propagating guided Lamb waves in the 3DCSS is multi-modal in nature with existence of four independent GW modes (A0, S0, A1 and S1) at 100 kHz frequency. The presence of BVLIDs in the structure substantially amplifies the A0 mode in the propagating GW signals. A good agreement was found between the numerical and experimental results for all the cases studied here. The proposed signal difference algorithm which works on the basis of change in A0 mode amplitude, has demonstrated its potential to efficiently localize the BVLID region in the structure within a network of PTDs. However, it is expected that the presence of baseline signal data may improve the inspection capability of the proposed technique. The future research will involve the development of baseline-free BVLID detection algorithms using the proposed SHM strategy.

ACKNOWLEDGEMENT

This research work was funded by the Polish National Science Centre (NCN) under Grant Agreement Number – UMO-2016/23/N/ST8/01326.

REFERENCES

- [1] D. Backstöm, A. Nilsson. Modeling flexural vibration of a sandwich beam using modified fourth-order theory. *Journal of Sandwich Structures & Materials*, **8**(6): 465–76, 2006.
- [2] H. Baid, C. Schaal, H. Samajder, A. Mal. Dispersion of Lamb waves in a honeycomb composite sandwich panel. *Ultrasonics*, **56**: 409–416, 2015.
- [3] S. Banerjee, C.B. Pol. Theoretical modeling of guided wave propagation in a sandwich plate subjected to transient surface excitations. *International Journal of Solids and Structures*, **49**(23): 3233–41, 2012.
- [4] M. Castaings, B. Hosten. Guided waves propagating in sandwich structures made of anisotropic, viscoelastic, composite materials. *The Journal of the Acoustical Society of America*, **113**(5): 2622–34, 2003.
- [5] G.A. Davies, D. Hitchings, J. Ankersen. Predicting delamination and debonding in modern aerospace composite structures. *Composites Science and Technology*, **31**: 846–54, 2006.
- [6] J. Fatemi, M.H.J. Lemmen. Effective thermal/mechanical properties of honeycomb core panels for hot structure applications. *Journal of Spacecraft and Rockets*, **46**: 514–525, 2009.
- [7] T.R. Hay, L. Wei, J.L. Rose, T. Hayashi. Rapid inspection of composite skin honeycomb core structures with ultrasonic guided waves. *Journal of Composite Materials*, **37**(10): 929–39, 2003.
- [8] F. He, Z. Zhou, Z. Feng. Research on an inspection method for de-bond defects in aluminum skin-honeycomb core sandwich structure with guided waves. In: *17th World Conference on Nondestructive Testing*, 25–28 Oct., Shanghai, China, 2008.
- [9] B. Lamboul, B. Passilly, J.-M. Roche, D. Osmont. Impact damage detection in sandwich composite structures using Lamb waves and laser vibrometry. In: *AIP Conference Proceedings*, Vol. 1511, No. 1, pp. 1003–1010, AIP, Jan. 25th, 2013.
- [10] L. Liu, K. Bhattacharya. Wave propagation in a sandwich structure. *International Journal of Solids and Structures*, **46**(17): 3290–300, 2009.
- [11] M.J. Lowe, R.E. Challis, C.W. Chan. The transmission of Lamb waves across adhesively bonded lap joints. *The Journal of the Acoustical Society of America*, **107**(3): 1333–45, 2000.
- [12] D.G. Luchinsky, V. Hafiychuk, V.N. Smelyanskiy, S. Kessler, J. Walker, J. Miller, M. Watson. Modeling wave propagation and scattering from impact damage for structural health monitoring of composite sandwich plates. *Structural Health Monitoring*, **12**(3): 296–308, 2013.
- [13] K. Maslov, T. Kundu. Selection of Lamb modes for detecting internal defects in composite laminates. *Ultrasonics*, **35**(2): 141–50, 1997.
- [14] Z. Mikulik. *Application of Fracture Mechanics to Predict the Growth of Single and Multilevel Delaminations and Disbonds in Composite Structures*. School of Mechanical and Manufacturing Engineering, University of New South Wales, Sydney, Oct. 2008.
- [15] S. Mustapha, L. Ye. Propagation behaviour of guided waves in tapered sandwich structures and debonding identification using time reversal. *Wave Motion*, **57**: 154–70, 2015.
- [16] A. Nosier, R.K. Kapania, J.N. Reddy. Free vibration analysis of laminated plate using a layerwise theory. *AIAA Journal*, **31**: 2335–46, 1993.
- [17] W. Ostachowicz, P. Kudela, M. Krawczuk, A. Zak. *Guided waves in structures for SHM: the time-domain spectral element method*. John Wiley & Sons, Dec. 30th, 2011.
- [18] L. Pieczonka, P. Ukowski, A. Klepka, W.J. Staszewski, T. Uhl, F. Aymerich. Impact damage detection in light composite sandwich panels using piezo-based nonlinear vibro-acoustic modulations. *Smart Materials and Structures*, **23**(10): 105021, 2014.
- [19] U. Polimeno, M. Meo. Detecting barely visible impact damage detection on aircraft composites structures. *Composite structures*, **91**(4): 398–402, 2009.
- [20] U. Polimeno, M. Meo, D.P. Almond, S.L. Angioni. Detecting low velocity impact damage in composite plate using nonlinear acoustic/ultrasound methods. *Applied Composite Materials*, **17**(5): 481–8, 2010.
- [21] P. Qiao, M. Yang. Impact analysis of fiber reinforced polymer honeycomb composite sandwich beams. *Composites Part B: Engineering*, **38**(5): 739–50, 2007.
- [22] R. Růžek, R. Lohonka, J. Jironč. Ultrasonic C-Scan and shearography NDI techniques evaluation of impact defects identification. *NDT & E International*, **39**(2): 132–42, 2009.
- [23] S. Sikdar, S. Banerjee, S.M. Subhani. Detection of disbond in a honeycomb composite sandwich structure using ultrasonic guided waves and bonded PZT sensors. In: *Proceedings of the 14th Asia Pacific Conference on Nondestructive Testing*, Nov. 2013.

- [24] S. Sikdar, S. Banerjee. Identification of disbond and high density core region in a honeycomb composite sandwich structure using ultrasonic guided waves. *Composite Structures*, **152**: 568–78, 2016.
- [25] F. Song, G.L. Huang, K. Hudson. Guided wave propagation in honeycomb sandwich structures using a piezoelectric actuator/sensor system. *Smart Materials and Structures*, **18**(12): 125007, 2009.
- [26] S.V. Sorokin. Analysis of propagation of waves of purely shear deformation in a sandwich plate. *Journal of Sound and Vibration*, **291**(3): 1208–20, 2006.
- [27] B. Wang, L. Wu, X. Jin, S. Du, Y. Sun, L. Ma. Experimental investigation of 3D sandwich structure with core reinforced by composite columns. *Materials & Design*, **31**: 158–65, 2010.
- [28] B. Xu, V. Giurgiutiu. Single mode tuning effects on Lamb wave time reversal with piezoelectric wafer active sensors for structural health monitoring. *Journal of Nondestructive Evaluation*, **26**(2): 123–34, 2007.
- [29] X. Zhao, H. Gao, G. Zhang, B. Ayhan, F. Yan, C. Kwan, J.L. Rose. Active health monitoring of an aircraft wing with embedded piezoelectric sensor/actuator network: I. Defect detection, localization and growth monitoring. *Smart Materials and Structures*, **16**(4): 1208, 2007.